A New Method to Resolve X-Ray Halos around Point Sources with *Chandra* Data and Its Application to Cygnus X-1

Yangsen Yao, S. Nan Zhang, Xiaoling Zhang & Yuxin Feng
University of Alabama in Huntsville, National Space Science and Technology Center

Abstract

With excellent angular resolution, good energy resolution and broad energy band, the *Chandra* Advanced CCD Imaging Spectrometer (ACIS) is the best instrument for studying the X-ray halos around some Galactic X-ray point sources caused by the dust scattering of X-rays in the interstellar medium. However, the direct images of bright sources obtained with ACIS usually suffer from severe pile-up. Making use of the fact that an isotropic image could be reconstructed from its projection into any direction, we can reconstruct the images of the X-ray halos from the data obtained with the High Energy Transmission Grating Spectrometer (HETGS) and/or in Continuous Clocking (CC) mode. These data have no or less serious pile-up and enable us to take full advantage of the excellent angular resolution of Chandra. With the reconstructed high resolution images, we can probe the X-ray halos as close as $1''$ to their associated point sources. Applying this method to Cygnus X-1 observed with Chandra HETGS in CC mode, we derived an energy dependent radial halo flux distribution and concluded that, in a circular region ($2'$ in radius) centered at the point source: (1) relative to the total intensity, the fractional halo intensity (FHI) is about 15% at ∼1 keV and drops to about 5% at ∼6 keV; (2) about 50% of the halo photons are within the region of a radius less than $40''$; and (3) the spectrum of the point source is slightly distorted by the halo contamination.

Introduction

The existence of the dust scattering X-ray halos was first discussed by Overbeck (1965) and was first observationally confirmed by Rolf (1983) using the data of GX339-4 with IPC/Einstein. Using HRI/Einstein, Catura (1983) and Bode et al.(1985) also confirmed the existence of X-ray scattering halos around point sources GX 3+1, GX 9+1, GX 13+1, GX 17+2 and Cygnus X-1. The recent main results on X-ray halo studies were reported by Predehl & Schmitt (1995) by systematically examining 25 point sources and 4 supernova remnants with ROSAT observations.

However, because the differences between halo profiles from different spatial distributions and dust models are significant only in the core of the halo (Figure 1, Figure 2, Mathis & Lee 1991), the limited angular resolutions of previous instruments ($1'$ for IPC/Einstein and $25''$ for PSPC/ROSAT) prevent the previous works from probing regions close to the point sources, and make it difficult to study the properties of the dust grains and to distinguish between various dust models observationally (Predehl & Klose 1996).

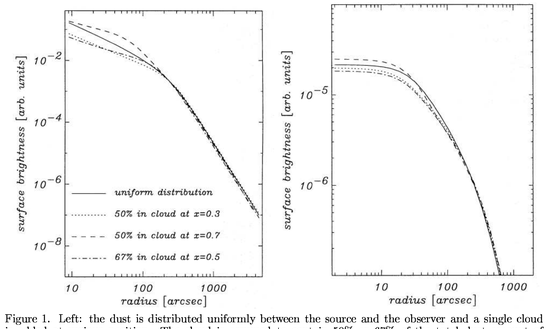

Figure 1. Left: the dust is distributed uniformly between the source and the observer and a single cloud is added at various position. The cloud is assumed to contain 50% or 67% of the total dust amount of the line of sight. Right: MRN distribution with a_{max} = 0.25 μm, uniformly distributed between x=0 and x=0.95 has been assumed. Curves are for different optical depths τ_{sca}=0.3(dotted), τ_{sca}=0.6(dashed), and τ_{sca}=1.2(dotted/dashed). The solid line is for the single scattering case. The photon energy is 1.5 keV (Predehl & Klose 1996).

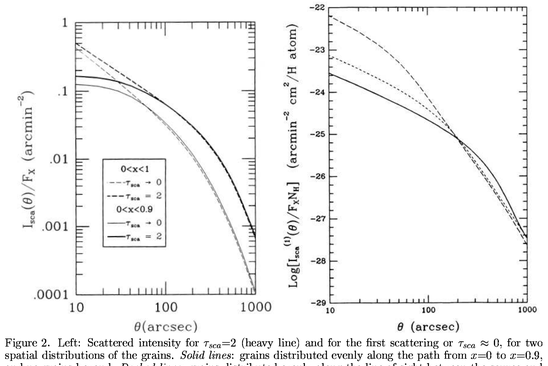

Figure 2. Left: Scattered intensity for τ_{sca}=2 (heavy line) and for the first scattering or $\tau_{sca} \approx 0$, for two spatial distributions of the grains. *Solid lines*: grains distributed evenly along the path from x=0 to x=0.9, and no grains beyond. *Dashed lines*: grains distributed evenly along the line of sight between the source and the observer. The energy is 1 keV (Mathis & Lee 1991).

The Advantage of *Chandra*

The Advanced CCD Imaging Spectrometer (ACIS) aboard the *Chandra X-ray Observatory*, with its excellent angular resolution, broad energy band and reasonably good energy resolution, is the most promising instrument to date in the X-ray halo study. However, the timed exposure (TE) mode of ACIS (providing a two-dimensional image) often suffers from severe pile-up, therefore, it is difficult to estimate the source flux and the halo profile near the point source in this case (see, e.g., Smith, Edgar & Shafer 2002). ***Because only bright sources can generate significant X-ray scattering halos, and observations of bright sources with ACIS/Chandra TE mode always suffer from severe pile-up, the excellent spatial resolution of Chandra has not brought the anticipated breakthrough to X-ray halo study.***

The pile-up can be avoided or lessened via operating in the Continuous Clocking (CC) mode and/or using the transmission grating. However, the CC mode data only provide one-dimensional intensity distribution. The TE grating data, though provide two-dimensional information, are already dispersed by the grating instruments.

Method and Simulation

Because of the grating principle, $p \sin\beta = m\lambda$, the zeroth order image (m = 0) is the same as the direct image except for a smaller flux. For a mono-energy source, the *Chandra* transmission grating will detect exactly the same intensity distribution in its higher order images as in its zeroth order image, as long as the source size is not too large (less than $3'$), as shown in Figure 3. If we project the secondary and higher order photons to a line perpendicular to the grating arm, the projected one-dimensional image will be the same as the projection of the zeroth order image. Because the grating only diffracts photons along the direction of the grating arm, the above projection is also valid for sources with continuum spectra. Usually the non-zeroth order grating images and the CC mode data have no or much less pile-up; either of them can be used to reconstruct the original image.

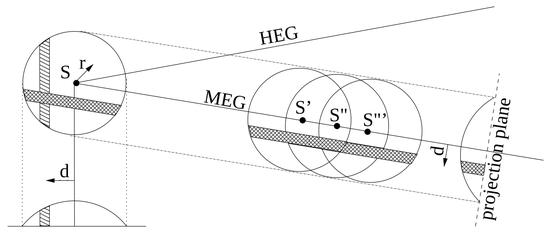

Figure 3. The projection of the photons along the grating arm and the projection of the photons in zeroth order image along an arbitrary direction.

If the flux of a point source plus its X-ray halo is isotropically distributed and centered at the point source as $F(r)$, and the projection process described above can be represented by a matrix operator $M(r,d)$, then the projected flux distribution $P(d)$ is

$$P(d) = F(r) \times M(r,d),$$

where r is the distance from the centroid source position and d is the distance from the projection center (refer to Figure 3). The inverse matrix of the operator $M(r,d)$ exists, and the original distribution can be easily resolved. We used numerical integration to approach the above projection process and built a matrix to approximate the integration and calculate $M(r,d)^{-1}$.

To test our method, we produced with MARX simulator a point source plus two disk sources to mimic a point source with its X-ray halo observed with *Chandra*/HETGS in TE mode. Using the intrinsic CCD energy resolution, we extracted the photons in the energy range 1.0–1.5 keV and performed the test in this energy band. We projected the zeroth order photons along an arbitrary direction to mimic the CC mode, projected the MEG photons along the MEG grating arm, and then multiplied these projected flux distribution with $M(r,d)^{-1}$ to resolve the flux distributions of the point source plus its halo. The reconstructed halo surface brightness distribution is consistent with the simulation input, as shown in Figure 4, so is the FHI, with the input value of 27.7% and the recovered value of 25.5%.

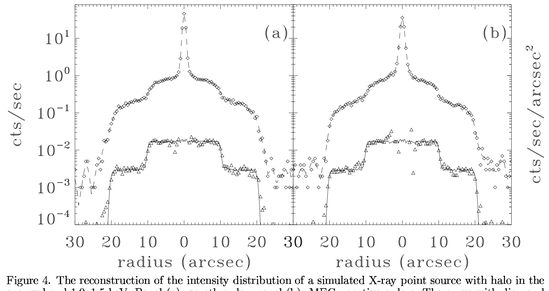

Figure 4. The reconstruction of the intensity distribution of a simulated X-ray point source with halo in the energy band 1.0–1.5 keV. Panel (a): zeroth order; panel (b): MEG negative orders. The curve with diamond symbols and the dashed line are the projected photon distribution (cts/sec). The triangle symbols are for the reconstructed halo distribution (cts/sec/arcsec^2), after subtracting the PSF of the point source. The solid line is the halo distribution from the zeroth order image of the simulated halo (no pile-up in the simulation).

Application to Cygnus X-1

We applied our method to the CC mode data of Cygnus X-1 observed on 2000 January 12 (ObsID 1511) with effective exposure of 12.7 ks. We used the zeroth order data within $2'$ from the source position. For energies above 3.0 keV, we use an exponential function to interpolate across the gaps caused by mis-identifying the halo photons as grating events. The estimated pile-up is 23% (PIMMS). To estimate the point source flux more accurately, we compared the grating data of the short-frame observation on 1999 October 19 with the grating data of this CC mode observation, then used the read-out streak of the short-frame to infer the point source flux at different energy bands (with width 0.5 keV). We also use MARX to obtain the piled-up PSFs for different energy bands.

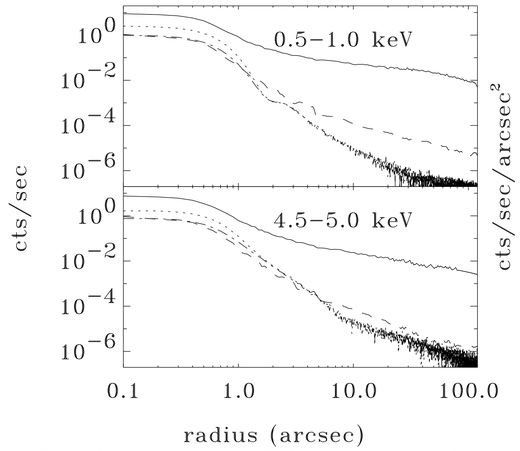

Figure 5. The flux distribution of Cygnus X-1 and the PSF in two energy bands. In each panel, the solid line indicates the projected flux distribution (cts/sec), and the other lines are for flux distributions (cts/sec/arcsec^2). *Dashed line*: source with halo; *dotted line*: PSF; *dash – dotted line*: piled-up PSF.

The reconstructed flux distributions are shown in Figure 5 (only two energy bands for demonstration). Even though there is pile-up in the core region, the halo can be clearly resolved down to $1''$ from the point source in the 0.5–1.0 keV band. The fractional halo intensity is shown in Figure 6(a); the fraction drops from about 15% around 1 keV to about 5% around 6 keV. We define the half-flux radius $R_{0.5}$ of the halo as the radius which encloses half of the halo photons in the $2'$ region. The half-flux radius $R_{0.5}$ is shown in Figure 6(b); clearly 50% of the halo photons are concentrated within $40''$. We also investigated how the halo contaminated the point source spectrum in Cygnus X-1 (see Figure 6(c) and Figure 6(d)). The halo spectrum is softer than the point source spectrum, especially in the low energy band (below 3 keV). Contributing only ∼ 10% to the total brightness, the X-ray halo in Cygnus X-1 does not distort the original point source spectrum significantly.

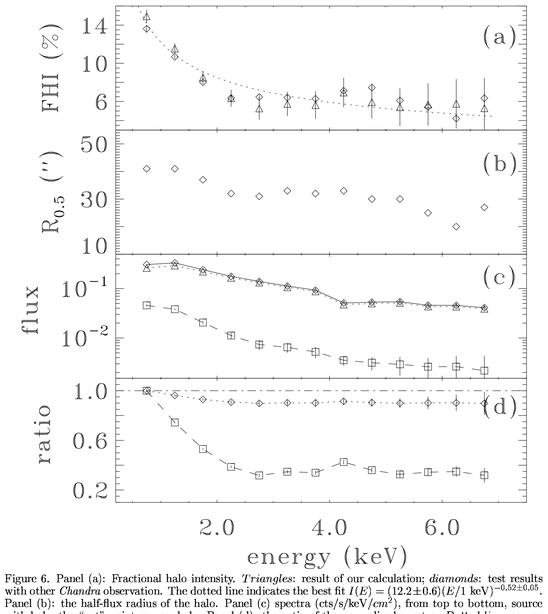

Figure 6. Panel (a): Fractional halo intensity. *Triangles*: result of our calculation; *diamonds*: test results with other *Chandra* observation. The dotted line indicates the best fit $I(E) = (12.2 \pm 0.6)(E/1\ \mathrm{keV})^{-0.52 \pm 0.05}$. Panel (b): the half-flux radius of the halo. Panel (c) spectra (cts/s/keV/cm^2), from top to bottom, source with halo, the "net" point source, halo. Panel (d): the ratio of the normalized spectra. *Dotted line*: source with halo to "net" point source; *dashed line*: halo to "net" point source.

Conclusions and Discussion

We propose a new method to reconstruct the image of an X-ray point source with its associated X-ray scattering halo from the CC mode data and/or grating data. With this method and the high angular resolution of the *Chandra X-ray Observatory*, we are able to probe the intensity distribution of the X-ray halos as close as $1''$ to their associated point sources. This method is tested with the MARX simulation and applied to Cygnus X-1.

The derived fractional halo intensity is energy dependent, but does not seem to follow the E^{-2} law. This may be due to the limited region we used (within $2'$), because of the following two reasons: (1) the scattering optical depth $\tau_{sca} \propto E^{-2}$ was derived by integrating over all solid angles (Mathis & Lee 1991), instead of the $2'$ region we used; and (2) for single-scattering the mean scattering angle is related to energy as E^{-1} (Mathis & Lee 1991). In the low energy band, the fractional halo intensity we obtained are reasonably consistent with the value reported by Predehl et al.(1995) (11% at the ROSAT energy range 0.1–2.4 keV).

The existence of the halo around a point source might distort the spectrum of the point source, because the cross-section of the scattering process in the ISM is energy dependent. Since the previous instruments are unable to resolve the point source from the halo, many of the measurements of the continuum X-ray spectra of Galactic X-ray sources with significant X-ray scattering halo may suffer from this problem. Despite of no significant spectral distortion in Cygnus X-1 system (only about 10% halo), systematic studies of the X-ray halo distribution in the broad band should be carried out for other X-ray sources with significant X-ray scattering halos, before we can draw any conclusion on the significance of the halo induced distortion to their X-ray continuum spectra.

The spatial distribution of the dust grains is very important in interpreting the physical properties of the grains. The core region of an X-ray halo is sensitive to the spatial distribution, whereas the wings are not sensitive to the dust distributions (Predehl & Klose 1996; Mathis & Lee 1991). Because we can resolve the X-ray halos as close as $1''$ to the point sources, it is possible to determine the grain spatial distributions. Even though the grain size distribution and multiple-scatterings may reduce the differences between halo profiles from various spatial distributions, this degeneracy can be easily resolved by drawing the diagnostic diagram (Figure 7) proposed by Mathis & Lee (1991).

Systematically checking the halo contamination to the point source spectrum and constraining the different halo models will be our next work.

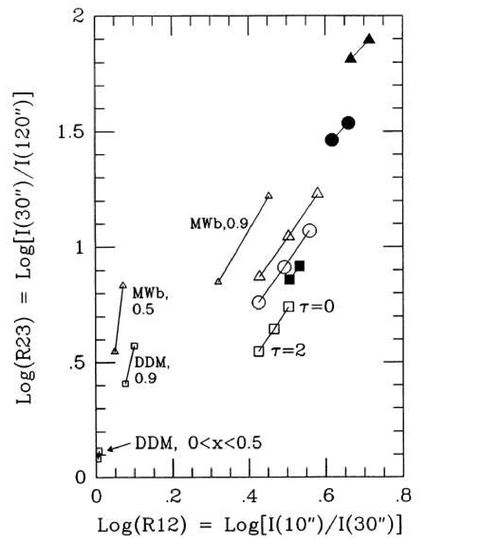

Figure 7. Ratio log(R12)=log[$I_s ca(10'')/I_s ca(30'')$], plotted against log(R23)=log[$I_s ca(30'')/I_s ca(120'')$], for scattering with various grain models, distribution of dust along the line of sight, and τ_{sca}. One each line, the upper endpoint is τ_{sca}=2; the lower τ_{sca}=0 (single scattering only). Some lines have the τ_{sca}=1 point marked as well. *Open symbols*: E=1 keV; *filled symbols*: E=2 keV for the same column density of grains. *Square*: the DDM model: *circles*: the Mathis & Whiffen (1989) mode A (for diffuse dust); *triangles*, the Mathis & Whiffen model for dense-cloud dust; *Large symbols*: uniform distribution of grains along the entire path; *small symbols*: distributions between the observer and X_{max}, with the value of X_{max} identified near the line (Mathis & Lee 1991).

REFERENCES

Bode, M. F., Pricdhorsky, W. C., Norwell, G. A. & Evans, A. 1985, ApJ, 299, 845
Catura, R. C. 1983, ApJ, 275, 645 Hayakawa, S. 1970, Progr. Theor. Phys., 43, 1224
Mathis, J. S. & Lee, C.-W. 1991, ApJ, 376, 490
Mathis, J. S., Rumpl, W. & Nordsieck, K. H. 1977, ApJ, 217, 425
Martin, P. G. & Sciama, D. W. 1970, Ap. Letters, 5, 193
Overbeck, J. W. 1965, ApJ, 141, 864
Predehl, P. & Klose, S. 1996, A&A, 306, 283
Predehl, P. & Schmitt, J. H. M. M. 1995, A&A, 293 889
Rolf, D. P. 1983, Nature, 302, 46
Smith, R. K., Edgar, R. J. & Shafer, R. A. 2002, ApJ, 581, 562